Indian Journal of Pure & Applied Physics
Vol. 62, April 2024, pp. 285-291
DOI: 10.56042/ijpap.v62i4.7614

On the Electrical and Thermal Study of a MgZnO/ZnO HEMT for High Field Applications

Saheb Chakraborty[a,b], Radha Raman Pal[b] & Sutanu Dutta[c*]

[a]Department of Physics, Garhbeta College, West Bengal, 721 121, India

[b]Department of Physics, Vidyasagar University, West Bengal,721 102, India

[c]Department of Electronics, Vidyasagar University, West Bengal,721 102, India

Received 28 December 2023; accepted 5 February 2024

In this work, a simple current equation of a HEMT based on MgZnO and ZnO heterojunction is proposed in the framework of electron velocity saturation. The mathematical formulation of drain current is presented as a function of mole fraction and device temperature. It is observed that the effect of the mole fraction of MgZnO has a significant role to modulate the drain current of the device. For example, the drain current is shifted by almost 9% for a change in mole fraction from 0.2 (236.5mA) to 0.5 (257.2mA) when no gate voltage is applied. In addition to this, the impact of environmental thermal variation is included in our study and a noticeable shift of drain current and other device parameter has been observed for a temperature range 300K to 500K. This work has also been extended to study the switching characteristics of the device in terms of mole fraction of MgZnO and ambient temperature. It is observed that the threshold voltage is shifted by 0.36 V for a change in mole fraction by 0.2.

Keywords: ZnO MODFET; ZnO HEMT; Velocity saturation model; DC characteristics; RF characteristics; MgZnO/ZnO heterostructure

1 Introduction

High Electron Mobility Transistors (HEMTs) based on MgZnO-ZnO heterojunction becomes very popular to the new generation researchers. This is due to the exciting material properties of ZnO such as wide energy band gap (3.37 eV), high saturation electron velocity (3.2×10^7 cm/s), high critical electric field *etc.*[1-5]. Further its direct band gap enables itself to be a good semiconductor material for optoelectronic applications. It is non-toxic, eco-friendly and transparent material when it is in pure form. Moreover, it is radiation-hard material and hence it can be used in electronic devices to operate in satellites in low earth orbits. Besides the minimum lattice mismatch of MgO and ZnO and large tunable band gaps enable itself to provide a good heterojunction structure[6-10].

A number of works have been done earlier to study the performance of ZnO HEMT[11-15]. Verma *et al*. derived an expression of 2DEG density with respect to gate voltage at the hetero-interface by solving the 1D Schrodinger's equation in the triangular potential well[11]. In a very recent work they have also studied the electrical performance of the device using a physics based analytical model and calculated various device parameters[12]. In another work, they have simplified the expression for Fermi energy level to develop a 2D analytical model for 2DEG density and hence to develop the I-V characteristics of HEMT[13]. Singh *et al*. developed an analytical model of two dimensional electron gas density and threshold voltage for a fully strained graded MgZnO/ZnO heterostructure with cap layer[14]. Kumar *et al*. developed an analytical model to explain the power switching characteristics of ZnO based HEMTs[15]. In a very recent work we have developed a theoretical model of MgZnO/ZnO HEMT considering accurate velocity field relation of ZnO[16]. The theoretical works on ZnO HEMTs reported so far are limited and there is a good scope to work on it. For short channel devices when the gate length of the device is considerably small, the drain field becomes higher even if a low drain bias is applied. In such cases the device is subjected to high drain field and the velocity of the electrons is near to its saturation value. In this scenario, the velocity saturation model is appropriate to find out the device current. But, in the previous works reported so far, the issue of electron velocity

*Corresponding author: (E-mail: sutanu@mail.vidyasagar.ac.in)

saturation was not addressed properly. In our work, we have developed a simple but attractive model to find the drain current in the device under the purview of electron velocity saturation. This model is best suited for high power and high field applications. Another important issue of interest is the impact of mole fraction on the device performance and the impact of environmental temperature. However, all these issues are integrated in this work and the performance of the device is studied accordingly. In addition, we have calculated thermal sensitivities of different device parameters to study the thermal impact of the device more precisely and accurately.

2 Drain Current Formulation

The schematic diagram of MgZnO/ZnO HEMT is shown in Fig. 1(a & b) shows the corresponding energy band diagram of the device. Here, $q\emptyset_b$ represents the barrier height of the metal semiconductor junction at the gate.

ΔE_C is the band gap energy difference between MgZnO and ZnO. d_1 is the thickness of n-MgZnO layer, d_0 corresponds to the undoped MgZnO layer and Δd is the thickness of the inversion layer.

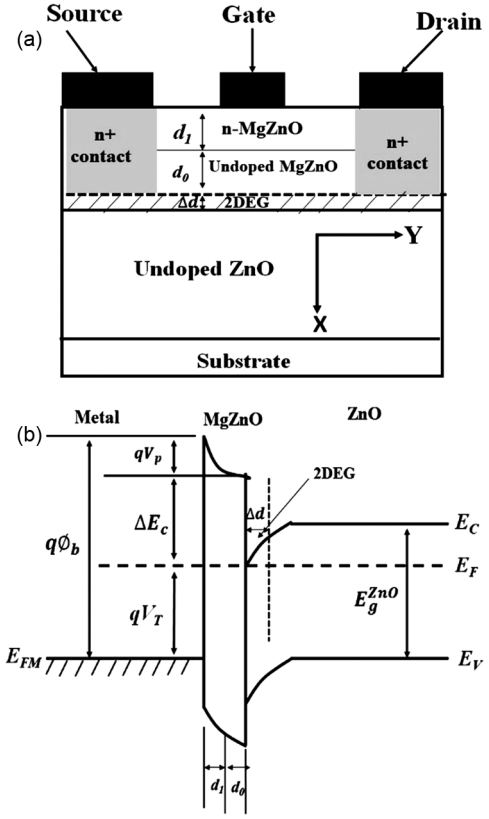

Fig. 1 — (a) A schematic diagram of MgZnO/ZnO HEMT (b) Energy band diagram of a MgZnO/ZnO heterojunction.

The threshold voltage of the device can be calculated from the energy band diagram as presented in Fig. 1(b) and is given by[17]

$$\left.\begin{aligned} V_T &= \emptyset_b - \frac{\Delta E_c}{q} - V_P \\ V_p &= \frac{qN_d d_1^2}{2\varepsilon} \end{aligned}\right\} \quad \ldots(1)$$

V_p is known as the pinch-off voltage of the device. N_d is the doping concentration in the n-MgZnO region and ε is the relative permittivity of MgZnO. We assume that the applied drain field is sufficiently high above the critical field required for electron velocity saturation in ZnO. In this situation, the drain current will follow the velocity saturation model and is given as follows[17]

$$\left.\begin{aligned} I_d &= Zv_sC_i[V_g - V_T - V_d(y)] \\ C_i &= \varepsilon/(d_1 + d_0 + \Delta d) \end{aligned}\right\} \quad \ldots(2)$$

Where, Z is the gate width, v_s represents the saturation velocity of electrons and C_i is defined as the sheet capacitance of the MgZnO and ZnO interface.

We assume that drain potential is uniformly distributed along the channel from source to drain. The drain bias at any distance 'y' from source to drain is given by

$$V_d(y) = \frac{yV_d}{L} \quad \ldots(3)$$

Where, L represents the channel length.

Considering the above assumption, the drain current can be calculated by integrating Eq. (2) from source to drain and is given as follows[18]

$$I_d = Zv_sC_i[V_g - V_T - V_d/2] \quad \ldots(4)$$

3 Dependence on mole fraction

The various material and device parameters such as relative permittivity, barrier height and the energy band gap of MgZnO are dependent on mole fraction and their functional dependence is given by[14]

$$\left.\begin{aligned} \epsilon(x) &= 8.75 + 1.08x \\ \emptyset_b(x) &= 5.81x^2 - 3.12x + 1.12 \\ E_g^{Mg_xZn_{1-x}O}(x) &= 3.37 + 2.145x \end{aligned}\right\} \quad \ldots(5)$$

Where, 'x' is the mole fraction.

4 Dependence on temperature

The energy band gap of ZnO changes with temperature and its functional dependence is given by[20]

$$E_g^{ZnO}(T) = E_g^{ZnO} - \frac{\Theta T^2}{T + T_1} \quad \ldots(6)$$

Table1 — Material and Device parameters used in calculations

Parameters	Value
N_d	3×10^{24} /m^3
Z	75 µm
L	0.1µm
d_1	17 nm
d_0	3 nm
Δd	5 nm
E_g^{ZnO}	3.37 eV
v_{s0}	3.2×10^5 m/s
T_0	300 K
T_1	310 K
a	1.581
b	-2.431×10^{-3} K^{-1}
c	1.35×10^{-6} K^{-2}
L_{gd}	0.1µm
L_{gs}	0.1µm
L_g	0.1µm
Θ	4.35×10^{-4} eV/K
α	1.43×10^{-4} eV/K

The values of E_g^{ZnO},Θ and T_1 are given in Table 1 and T corresponds to ambient temperature.

The energy band gap of MgZnO changes with temperature and its functional dependence as follows[10]

$$E_g^{Mg_xZn_{1-x}O}(T) = E_g^{Mg_xZn_{1-x}O}(x) - \frac{\alpha T^2}{T+T_0} \quad \ldots (7)$$

The values of T_0 and α are given in Table 1.

The thermal dependence of saturation velocity of the electron in ZnO is given by the Eq.[19]

$$v_s(T) = v_{s0}[a + bT + cT^2] \quad \ldots(8)$$

The values of the temperature coefficients v_{s0}, a, b and c are given in Table 1.

5 Mutual Conductance

The mutual conductance (g_m) of the device is calculated by differentiating drain current (I_d) in Eq. 4 with respect to gate voltage (V_g) at constant drain voltage and given by

$$g_m = Zv_sC_i \quad \ldots(9)$$

6 Drain Conductance

The drain conductance (g_d) of the device is calculated by differentiating drain current (I_d) in Eq. 4 with respect to drain voltage (V_d) at constant gate voltage

$$g_d = -\frac{Zv_sC_i}{2} \quad \ldots(10)$$

7 Cut-off Frequency

The Cut-Off Frequency of the device can be defined as

$$f_c = \frac{g_m}{2\pi ZLC_i} = \frac{v_s}{2\pi L} \quad \ldots(11)$$

8 Maximum operating frequency

$$\left.\begin{aligned} F_{max} &= \sqrt{\frac{F_c}{8\pi R_g C_{gd}}} \\ R_g &= \frac{L_g}{qN_dZd\mu_{MgZnO}} \\ C_{gd} &= \frac{\epsilon ZL_{gd}}{d_1+d_0+\Delta d} \end{aligned}\right\} \quad \ldots (12)$$

Where C_{gd} is the gate to drain capacitance, L_{gd} is the gate to drain length, R_g is the gate parasitic resistance, μ_{MgZnO} is the electron mobility of the MgZnO layer.

9 Thermal sensitivity

In order to understand the impact of ambient temperature on the device more preciously we calculate thermal sensitivities of various device parameters. The thermal sensitivity of a parameter (P) is the thermal derivative of that parameter P and is represented as S_P. Here we have calculated the thermal sensitivities of drain current, threshold voltage, cut-off frequency and maximum operating frequency of the device and are given as follows

$$S_{I_d} = \frac{dI_d}{dT} = \mathrm{Z}C_i\left[v_{s0}(b+2cT)\left(V_g - V_T - \frac{V_d}{2}\right) - v_sS_{V_T}\right] \quad \ldots(13)$$

$$S_{V_T} = \frac{dV_T}{dT} = \frac{\Theta T}{T+T_1}\left(2 - \frac{\mathrm{T}}{T+T_1}\right) - \frac{\alpha T}{T+T_0}\left(2 - \frac{\mathrm{T}}{T+T_0}\right) \quad \ldots(14)$$

$$S_{Fc} = \frac{dF_c}{dT} = \frac{v_{s0}(b+2cT)}{2\,\pi L} \quad \ldots(15)$$

$$S_{F_{max}} = \frac{dF_{max}}{dT} = \sqrt{\frac{1}{32F_c\pi R_gC_{gd}}} \quad \ldots (16)$$

10 Data Validation

The expression of drain current presented in Eq. 4 shows its dependence on various material and device parameters. Eqs. (5) to (8) presents the dependence of different material parameters on mole fraction and ambient temperature. The variation of the drain current with drain voltage is shown in Fig. 2. To validate our work it is required to compare our results with the experimental data. The experimental data on ZnO HEMT reported in literature are very rare. However, we find out an experimental work in reference[21] and compare it with the theoretical results

obtained for our calculation and it is presented in Fig. 2. It is observed that our results match pretty well with the data reported in[21]. The device structure and other parameters are considered to be equivalent to the device presented in reference[21].

11 Results and Discussion

In this section we have computed drain current and other device parameters using Matlab and these parameters are studied mostly with mole fraction and ambient temperature.

The variation of the drain current with drain voltage is shown in Fig. 3 for different values of mole fraction. The gate length is assumed as 0.1 μm and for an applied drain voltage of 2V, the electric field is 2×10^5 V/cm which is well above the critical field required for electron velocity saturation in ZnO. The graph shows that the drain current decreases with drain voltage but increases with mole fraction. This is due to the fact that after electron velocity is saturated, there is no scope to enhance the velocity of electrons with a further increase of drain bias. On the contrary, the 2D inversion layer charge density decreases with drain bias. As a result, drain current reduces with drain bias.

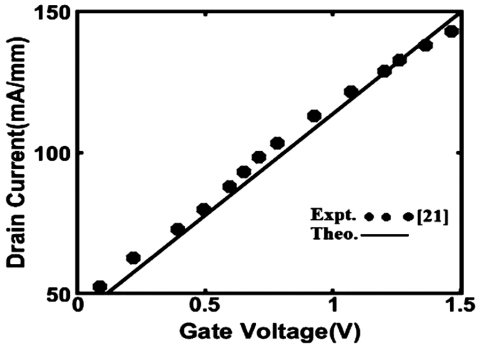

Fig. 2 — Variation of drain current with gate voltage for V_D=6V and mole fraction (x) =0.37.The material and device parameters used in the calculation are given in Table 1.

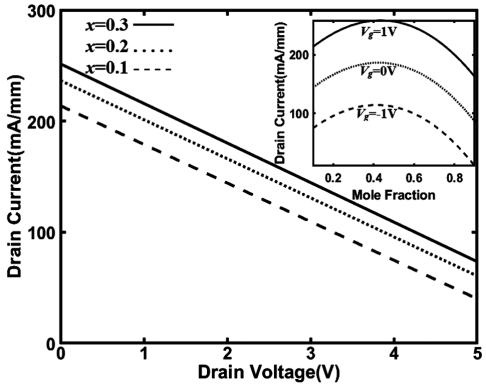

Fig. 3 — Variation of drain current with drain voltage for different mole fractions at V_G=0V. The variation of drain current with mole fraction for different gate voltages is shown in the inset. The material and device parameters used in the calculation are given in Table 1.

The figure in the inset of Fig. 3 shows the variation of drain current with mole fraction. The drain current first increases and then decreases with mole fraction. This is due to the fact that the wurtzite (WZ) structure of MgZnO is sustained up to the mole fraction x=0.37 and then its starts to change its form towards the rocksalt (RS) structure[22]. The MgZnO is in mixed-phase from the value of mole fraction of x=0.37 to x=0.62 and after it exceeds the value 0.62 it is totally converted to rocksalt (RS) and hence the drain current reduces. It is also observed that the drain current decreases with gate voltage.

Figure 4 shows the variation of drain current with temperature for different mole fractions. The drain current reduces with temperature because as the temperature raises the saturation velocity of the electrons decreases and hence the drain current decreases.

Figure 5 shows the variation of threshold voltage with temperature for different values of mole fraction. It is observed that, as the temperature is enhanced the

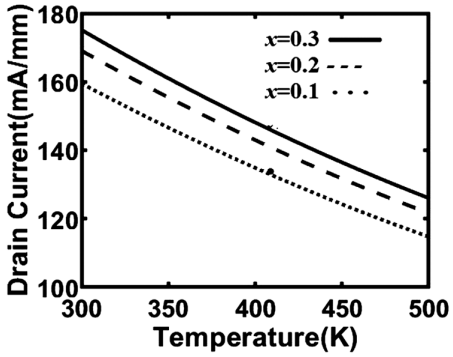

Fig. 4 — Variation of drain current with respect to temperature for different mole fraction. The material and device parameters used in calculations are given in Table 1.

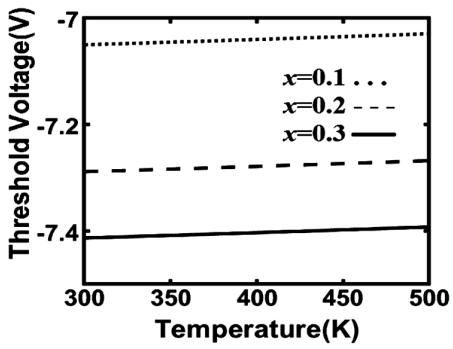

Fig. 5 — Variation of threshold voltage with temperature for different mole fractions. The material and device parameters used in the calculation are given in Table 1.

threshold voltage enhances. This is because drain current reduces with temperature and comparatively lower reverse bias is required to achieve the threshold condition of the device.

Figure 6 shows the variation of thermal sensitivity of threshold voltage with temperature. It is observed from the Figure that the sensitivity of threshold voltage increases with respect to temperature. S_{VT} is independent on other device parameters, such as mole fraction, barrier layer thickness, channel length *etc*. It is also observed from the figure that S_{VT} shows a very little variation of 0.03 mV/K over the temperature range 300K to 500K which reveals that the thermal sensitivity of threshold voltage is almost constant with temperature.

Figure 7 shows the variation of thermal sensitivity of drain current with respect to temperature for different values mole fraction. It is observed from Fig. 7 that S_{Id} almost varies linearly with respect to temperature. It results that the thermal variation of drain current is not constant rather shows a non-linear dependence. A small shift in sensitivity is observed for different mole fraction and it is lowest (close to zero) for low mole fraction. This result indicates that S_{Id} is minimum for x=0.1 which explores that the thermal impact on the device performance is minimum for low value of '*x*'.

Variation of cut off frequency with temperature is shown in Fig. 8. This figure shows that the cut off frequency decreases with temperature as the saturation velocity decreases with temperature. It is observed from the graph that the cut off frequency of the device reduces significantly with temperature and also with gate length. This is because when temperature increases the saturation electron velocity decreases. As a result of that the channel conductance of the device reduces. So cut off frequency of the device reduces due to low value of channel conductance at relatively higher temperature. In addition when gate length increases the resistance between source to drain increases that means the conductance of the channel reduces. On the other hand the electrons need more time to travel the distance from source to drain. As the time increases the frequency of the device must reduce.

The variation of thermal sensitivity of cut off frequency with temperature is shown in Fig. 9. It is

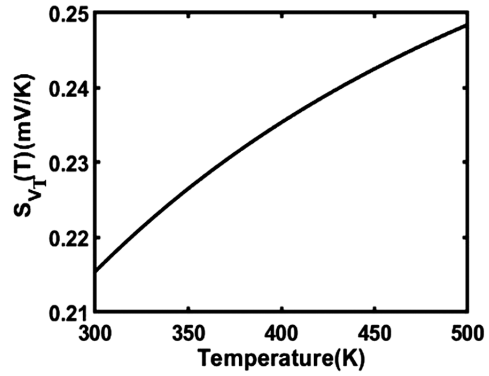

Fig. 6 — Variation of thermal sensitivity of threshold voltage with temperature. The material and device parameters used in the calculation are given in Table 1.

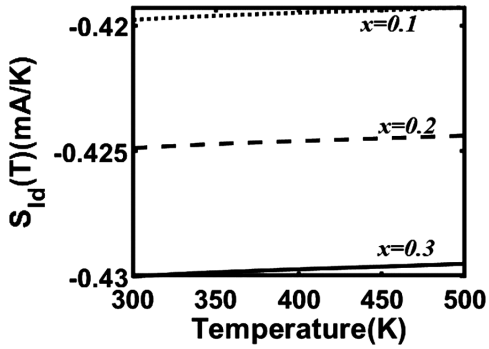

Fig. 7 — Variation of thermal sensitivity of drain current with temperature for different mole fraction. The material and device parameters used in calculation are given in Table 1.

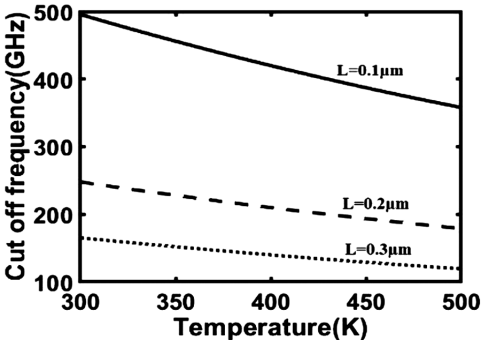

Fig. 8 — Variation of Cut off frequency with temperature for different gate length. The material and device parameters used in the calculation are given in Table 1.

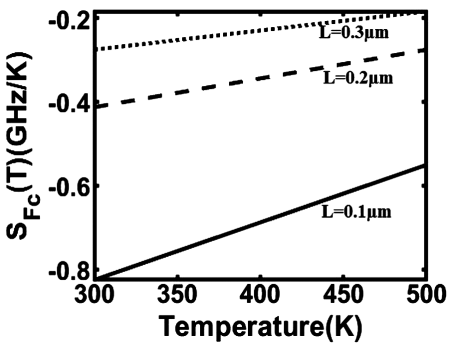

Fig. 9 —Variation of thermal sensitivity of cut off frequency with temperature for different gate length. The material and device parameters used in calculation are given in Table 1.

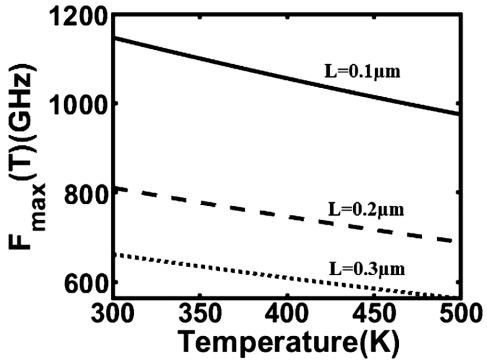

Fig. 10 — Variation of maximum operating frequency with temperature for different gate length. The material and device parameters used in the calculation are given in Table 1.

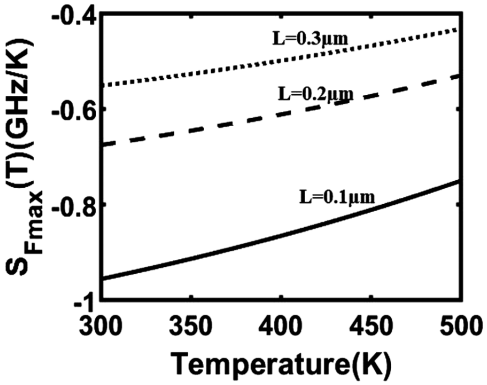

Fig. 11 — Variation of thermal sensitivity of maximum operating frequency with temperature for different gate length. The material and device parameters used in calculation are given in Table 1.

observed that the thermal sensitivity of cut off frequency moves towards zero when ambient temperature increases. It is also observed that the sensitivity is closer to zero when the channel length is high, so for the HEMTs applicable at high temperature region we should choose larger gate lengths so that the shift in cut-off frequency can be minimized.

The variation of maximum operating frequency with temperature is shown in Fig. 10. It is observed that the maximum operating frequency decreases with temperature and improves for smaller gate length. This is due to the fact that as gate length reduces the gate to source resistance decreases and hence maximum operating frequency increases.

Variation of thermal sensitivity of maximum operating frequency with temperature is shown in Fig. 11. It is observed that the sensitivity tends to zero if we increase the channel length. So for high temperature application we should prefer the devices having larger gate lengths to minimize the reduction of maximum operating frequency.

12 Conclusion

In this work, a current equation is developed to study the performance of MgZnO-ZnO HEMT operated under high electric field under the condition of electron velocity saturation. The current equation is simple and novel in order to study an MgZnO/ZnO HEMT. The device current significantly changes with mole fraction and ambient temperature. The device current reduces by 28 % for a change in temperature range from 300K to 500K. The drain current increases with mole fraction up to 0.5 and then it reduces as the structure of MgZnO (wurtzite or rockalt) depends on mole fraction. The values of S_{Id} are close to zero for low value of '*x*' although S_{VT} is independent of '*x*'. It is also observed that the value of S_{Fc} and S_{Fmax} is close to zero for higher value of '*L'*. This work has been extended to study the temperature sensitivities of various device parameters such as threshold voltage, drain current, cut off frequency and maximum operating frequency. Thus it can be concluded that the thermal impact on the device is less for low value of '*x'* and larger values of '*L'*.

References

1 Look D C, *Mater Sci Eng B*, 80 (2001) 383.
2 Look D C, *J Electron Mater*, 35 (2006) 1299.
3 Khan M A, Kumar P, Siddharth G, Das M & Mukherjee S, *IEEE Trans Electron Dev*, 66 (2019) 5097.
4 Choi S, Rogers D J, Sandana E V, Bove P, Teherani F H, Nenstiel C & Ton-That C, *Sci Rep*, 7 (2017) 7457.
5 Li Z, Wang P, He J, Chen H & Cheng J, *Superlatt Microstruct*, 111 (2017) 852.
6 Kozuka Y, Tsukazaki A & Kawasaki M, *Appl Phys Rev*, 1 (2014).
7 Ohtomo A, Kawasaki M, Koida T, Masubuchi K, Koinuma H, Sakurai Y & Segawa, Y, *Appl Phys Lett*, 72 (1998) 2466.
8 Šermukšnis E, Liberis J, Matulionis A, Avrutin V, Toporkov M, Özgür Ü & Morkoç H, *J Appl Phys*, 123 (2018).
9 Sasa S, Hayafuji T, Kawasaki M, Koike K, Yano M & Inoue M, *IEEE Electron Dev Lett*, 28 (2007) 543.
10 Zhou H P, Xu M & Shen W Z, *Phys B: Cond Matter*, 403 (2008) 3585.
11 Verma Y K, Mishra V & Gupta S K, *J Circuits, Syst Comput,* 29 (2020) 2050009.
12 Verma Y K & Gupta S K, *Micro Nanostruct*, 184 (2023) 207675.
13 Verma Y K, Mishra V, Verma P K & Gupta S K, *Int J Electron*, 106 (2019) 707.
14 Singh R, Khan M A, Mukherjee S & Kranti A, *IEEE Trans Electron Dev*, 64 (2017) 3661.
15 Kumar P, Chaudhary S, Khan M A, Kumar S & Mukherjee S, *Analytical Study of ZnO-based HEMT for Power Switching*, (2021).https://doi.org/10.21203/rs.3.rs-1140403/v1
16 Chakraborty S, Pal R R & Dutta S, *J Korean Phys Soc*, (2024). https://doi.org/10.1007/s40042-023-00985-6

17 Sze S M, *Semiconductor Devices Physics and Technology*, Wiley India Publication, (2011) 246.
18 Shit P, Pal R R & Dutta S, *AIP Conf Proc*, 2369 (2021).
19 Liu D, *J Comput Electron*, 1-9 (2023). https://doi.org/10.1007/s10825-022-01999-2
20 Alfaramawi K, *Bull Mater Sci*, 37 (2014) 1603.
21 Chaudhary S, Kumar P, Khan M A, Kumar A & Mukherjee S, *Eng Res Exp*, 4 (2022) 025007.
22 Zan Y H & Ban S L, *Superlatt Microstruct*, 150 (2021) 106782.